Steel and Composite Structures, *Vol. 37, No. 1* (*2020*) *15-26*
DOI: https://doi.org/10.12989/scs.2020.37.1.015

Experimental study on seismic behavior of exterior composite beam-to-column joints with large size stiffened angles

Peng Wang[1,2], Zhan Wang[1,3], Jianrong Pan*[1,3], Bin Li[1] and Bo Wang[1]

[1]*School of Civil Engineering and Transportation, South China University of Technology, Guangzhou 510641, China*
[2]*School of Civil Engineering and Transportation, Guangdong University of Technology, Guangzhou 510006, China*
[3]*State Key Laboratory of Subtropical Building Science, South China University of Technology, Guangzhou 510641, China*

(*Received July 3, 2019, Revised August 7, 2020, Accepted September 25, 2020*)

Abstract. The top-and-seat angles with double web angles are commonly used in the design of beam-to-column joints in Asian and North American countries. The seismic behavior analysis of these joints with large cross-section size of beam and column (often connected by four or more bolts) is a challenge due to the effects from the relatively larger size of stiffened angles and the composite action from the adjacent concrete slab. This paper presents an experimental investigation on the seismic performance of exterior composite beam-to-column joints with stiffened angles under cyclic loading. Four full-scale composite joints with different configuration (only one specimen contain top angle in concrete slab) were designed and tested. The joint specimens were designed by considering the effects of top angles, longitudinal reinforcement bars and arrangement of bolts. The behavior of the joints was carefully investigated, in terms of the failure modes, slippage, backbone curves, strength degradation, and energy dissipation abilities. It was found that the slippage between top-and-seat angles and beam flange, web angle and beam web led to a notable pinching effect, in addition, the ability of the energy dissipation was significantly reduced. The effect of anchored beams on the behavior of the joints was limited due to premature failure in concrete, the concrete slab that closes to the column flange and upper flange of beam plays an significant role when the joint subjected to the sagging moment. It is demonstrated that the ductility of the joints was significantly improved by the staggered bolts and welded longitudinal reinforcement bars.

Keywords: composite joints; beam-to-column connection; top and seat angles; seismic behavior

1. Introduction

The earthquake occurred in Northridge, and Hyogoken Nanbu caused severe damage in welded moment-resisting steel structures, particularly in the joints of the steel frame. Since then, bolted connections were suggested as an alternative connection types by various researchers. The top-and-seat angles with double web angles (TSDW) in beam-to-column joints that assembled with bolts are commonly used in structures in seismic-active areas such as East Asia and North America. This is because that such joints have considerable strength and initial stiffness, sufficient ductility, excellent energy-dissipation capacity and relatively low construction cost (Citipitioglu *et al*. 2002, Lee and Moon 2002, Garlock *et al*. 2003, Brunesi *et al*. 2014). The un-stiffened TSDW joints (a single row of two bolts is used on the un-stiffened tension angle leg) with regular size section has been widely studied over the past three decades (Pirmoz *et al*. 2009, Abdalla *et al*. 2015, Meng *et al*. 2018), these research outcomes have contributed to the development of design specifications, such as Eurocode 3 Part 1.8 (CEN-1993-1-8 2005) and Chinese Design Code of Steel Structure. (GB50017-2017 2018).

With the rapid development of structural technology in assembling in China, the larger size of structural members and the corresponding joints become more and more common in engineering construction, e.g., four bolts or more in a row in the assembling of beam-columns with stiffened angles, in this case, we call it large-size angles. Meanwhile, to enhance the structural performance of joints, the stiffener is commonly a better choice than increasing the angle thickness (Reinosa *et al*. 2015, Wang *et al*. 2018, Reinosa *et al*. 2019). However, previous research work has shown that the flexural characteristics of this type of connection are quite different from those of the non-stiffened TSDW joints due to the unique structure form Wang (2018).

Semi-rigid composite joints not only have the advantages of optimizing the use of materials but also have the benefit of providing lateral stiffness for the frame (Artar and Daloglu 2015). Such joints may provide lateral stability of the structure with adequate stiffness and ductility, hence, there is no need to use additional braces in the systems. These are widely used in composite structures. The experiences of Northbridge earthquake indicated that the composite effect of the floor in the structural systems with such joints must be considered in the structural analysis under seismic conditions. However, the seismic performance of this type of composite joints is different from the bare joints that most regular researches considered.

*Corresponding author, Professor
E-mail: ctjrpan@scut.edu.cn

ISSN: 1229-9367 (Print), 1598-6233 (Online)

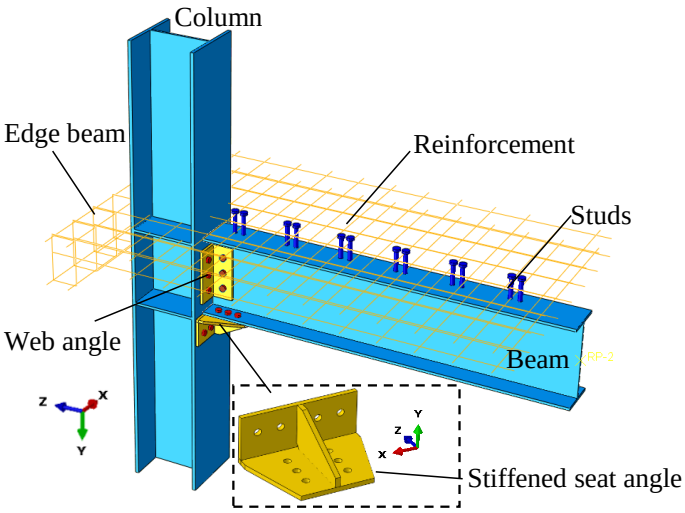

Fig. 1 Configuration of exterior composite beam-to-column joints with large size stiffened angle

A large number of experimental studies have been conducted on the composite semi-rigid joints, however, most of the research works were related to the monotonic and cyclic loading test of composite joints with extended and flush end-plates (Amadio and Fragiacomo 2003, Gil and Bayo 2008, Wang *et al*. 2018, Ma *et al*. 2019) or flange plate (Kumar and Smitha 2013, Lee *et al*. 2016). It should be noted that experimental investigation on the TSDW angle joints was relatively limited, such as Xiao *et al*. (1994) and Yuan *et al*. (2011), these researches just focused on the monotonic loading test in one direction only, but the structural performance of the composite joints under hogging and sagging moments are quite different due to effects from the concrete slabs. There are few studies focused on the hysteretic behavior, energy dissipation capacity and ductility index of the composite joints under cyclic loads, which are an indispensable basis for seismic design of structures. Hence, there is an imperative to carry out a further experimental study on this form of composite joints (as illustrated in Fig. 1) under cyclic loading conditions.

For exterior composite beam to column joints, the longitudinal reinforced bars are particularly critical in transferring horizontal force to column flange (Gil *et al*. 2013) and need to be anchored in spandrel beams or inside the concrete of column flange. In order to take into account the ease of construction and architectural function. Based on this fact, that longitudinally tension reinforced bars and compression concrete slab can replace part of the top angle's load-bearing function. Therefore, the large size stiffened angle steel on the upper beam flange (top angle) can be removed. A circular bolt pattern in extended plate connection can enhance the moment capacity, reduce pinching effect and energy-dissipation capacity (Kiamanesh *et al*. 2013, Hantouche and Mouannes 2016). There are also four bolts on one side of the large size stiffened angle connection. Thus, the above effects are considered in the specimen designs for the experimental investigation of this paper:

- Welding of the longitudinal reinforced bars.
- Presence of the large size stiffened angle steel on the upper beam flange.
- Bolt arrangements in angle leg connected to column flange.
- Anchored edge beam in exterior composite beam-to-column joints.

Hence, in this study, the seismic behavior and moment-rotation relationship of large size top-and-seat angles with double web angles composite joints were experimentally investigated. The purpose of this research work is to understand the performance of the exterior composite beam-column joints with stiffened angles under cyclic loading conditions and foster the application of this type of joints in composite frames.

2. Experimental program

2.1 Test specimens

To investigate the seismic behavior of exterior composite TSDW joints, a total of four types of joints with large size stiffened angles were designed and tested under cyclic loading to failure. The hot rolled steel column, steel beam, top-and-seat angles and web angles used in fabrication of all specimens were in Grade Q235B steel with the section of HW300×300×10×15, HN350×175×7×11, L200×125×12, and L100×100×12, respectively. The detailed configuration of the four specimens was illustrated in Fig. 2, the steel beam and column were assembled by high-strength bolts with a diameter of 16 mm. The bolts are of grade 10.9 having nominal yield strength of 900 MPa. They were tightened by electric torque spanner with a tension force of 100 kN, the diameter of the bolts was 16mm, corresponding to 18 mm holes were drilled in column, beam and angles, and the gap

Table 1 the design parameter of the four composite joints

Specimen ID	Top angle	Seat angle	Web angle	Reinforce bars	Bolt pattern
SJ-1	-	L200×125×12	L100×100×12	Cut off	Abreast
SJ-2	-	L200×125×12	L100×100×12	Welded	Abreast
SJ-3	L200×125×12	L200×125×12	L100×100×12	Cut off	Abreast
SJ-4	-	L200×125×12	L100×100×12	Cut off	Staggered

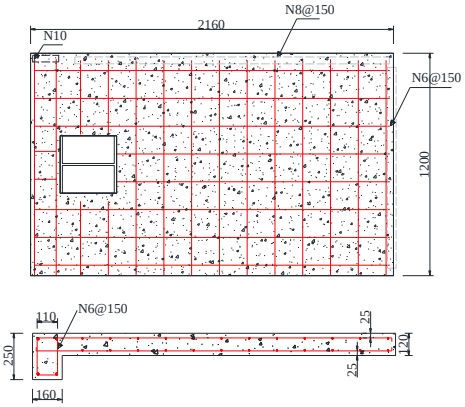

Fig. 2 Details of the concrete slab

between beam and column was 3 mm. The main design parameters are listed in Table 1. The specimen SJ-1 just has a stiffened seat angle, four high strength bolts are arranged abreast on the short leg of seat angle, the longitudinal reinforced bars were cut off in front of the column flange. The difference between specimen SJ-2 and SJ-1 is that the longitudinal reinforced bars were welded on the column flange. The specimen SJ-3 has top and seat angles and Staggered bolts were installed in stiffened seat angle of specimen SJ-4. The previous study (Wang *et al*. 2018) showed that triangular stiffeners produced local stress concentration. To minimize this effect, an improved stiffener is adopted in this research (as shown in Fig. 3).

Concrete Grade C30 was used in the double-layer reinforced concrete slab with a cover depth of 20 mm, the width, length, and thickness of the concrete slab were 1200 mm, 2160 mm and 120 mm, respectively. The longitudinal reinforced bars were set as 8@150. The bars were anchored in 250mm×160mm edge beam, he transverse bars were set as 6@150, as illustrated in Fig. 2. To meet the requirement of complete shear connection, the shear studs were designed with a height and diameter of 90 mm and 19 mm, respectively. The locations of the shear connectors are clearly illustrated in Fig. 3. The internal distance between adjacent studs was 40mm, and the spacing for every two studs was 200mm. There are 12 shear studs in a specimen of SJ-1, SJ-2, and SJ-4, and ten shear bolts are set in specimen SJ-3.

The Specimen SJ-1 which the top angle was removed and longitudinal reinforcement on the upper flange of the beam was cut off around the column face was used as standard one; The longitudinal reinforcements on the upper flange of the beam was welded to the face of column flange in Specimens SJ-2 as compared with that of Specimen SJ-1; the Specimen SJ-3 has a top-and-seat angle joint. In order to observe the deformation of the top angle, the upper space around of top angle wasn't covered with concrete to facilitate the observation of the deformation, meanwhile, the effect of concrete under sagging moment will be neglected; The difference between specimens SJ-4 and SJ-1 is that staggered bolt pattern was applied in seat angle of the specimen SJ-4. The configuration details and differences for different specimens are shown in Fig. 3.

2.2 Instrument

The tests of all the specimens were being conducted at The State Key Laboratory of Subtropical Building Science at the South China University of Technology. Fig. 4 schematically illustrates the test setup, the steel column ends were assembled by two hinges which could provide inflection point in the column of a steel frame, where one hinge was fixed in the floor, and the other one was connected and fixed on the reaction frame.

For all tests, the composite steel beam tip was loaded by an MTS series-100kN actuator that provided the vertical loading. The end of the actuator was fixed to the reaction frame. Cyclic vertical loads provided by MTS system were applied according to a displacement history based on the SAC loading protocol to represent deformation histories. The loading conditions are consistent with seismic demands in moment frame buildings (ANSI/AISC-341-16 2016). The

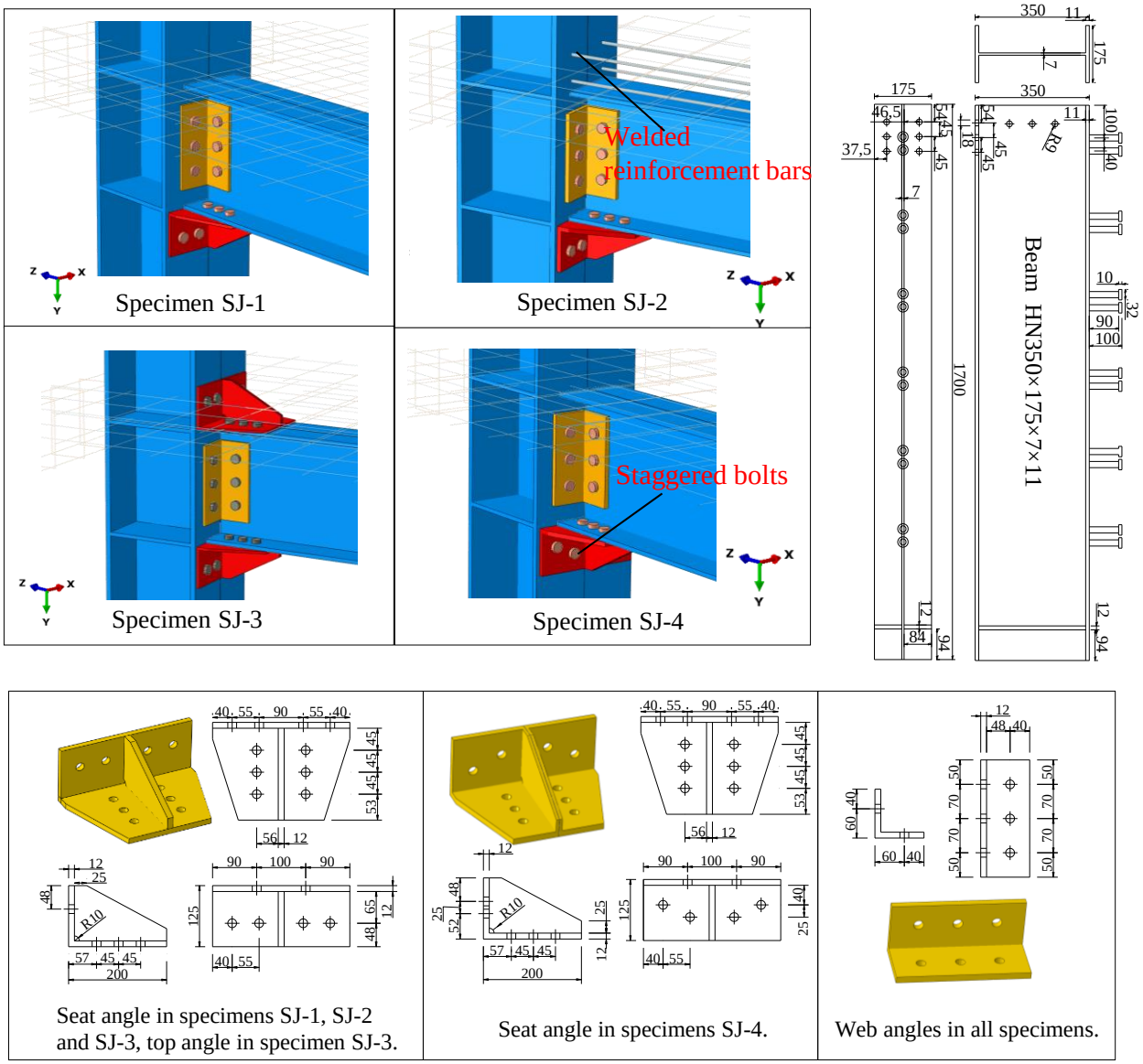

Fig. 3 Configuration of the specimens

loading procedure consisted of 14 stages. The displacement and the number of cycles at each stage are shown in Fig. 5. The drift angle can be represented by $\theta=v/L$, where v is the vertical distance recorded by MTS, L is the horizontal distance of the load cell center and the nearest outer face of the column flange. The first three loading stages were 0.375%, 0.5%, and 0.75% of story drift, for 6 cycles in each stage, followed by another two stages, namely, 4 cycles and 2 cycles for 1% and 1.5%, respectively. The rest of the nine loading stages started with 2% of story drift, two cycles for each stage. The test moment, $M=FL$, was calculated from the beam tip reaction force, F, multiplying the effective loading length of beams, L. Furthermore, a vertical axial load was applied through a hydraulic jack with an axial compression force to the top of the column end. The hogging and sagging moment were generated by the push and pull force of the vertical hydraulic jack, respectively.

In addition to the loads and displacements monitored by the actuator, instrumentations were installed on the specimen and loading frame to measure displacements, rotations, and strains (see Fig. 4). These instruments include position transducers attached to the steel column to measure the motion of the column. Strain gages were attached to the beam flange, beam web at several locations to monitor the beam yielding. Several strain gages were also installed on the surface of reinforcing bars; also, two uniaxial strain gages were attached to every anchor rod to measure axial rod strain.

2.3 Materials

The elastic modulus, yield strength, ultimate strength, and elongation of the steel specimens were determined by the material test. Tension tests were carried on steel

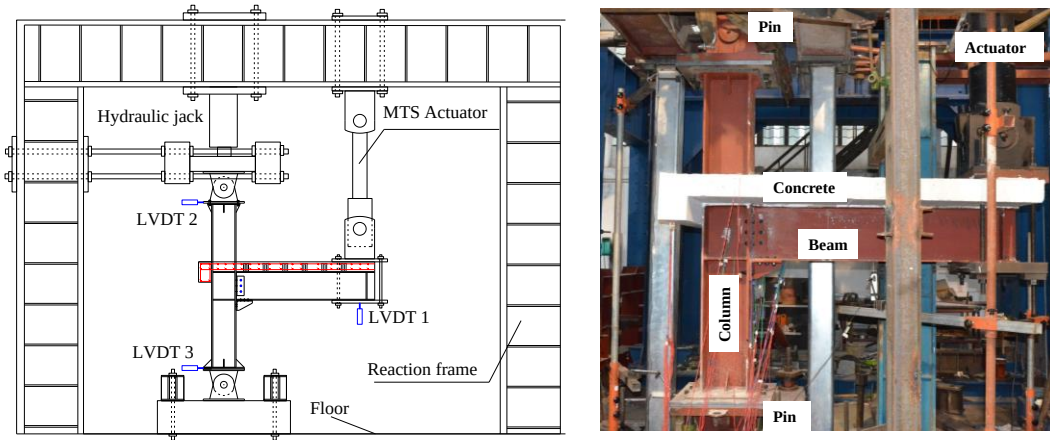

Fig. 4 Test setup

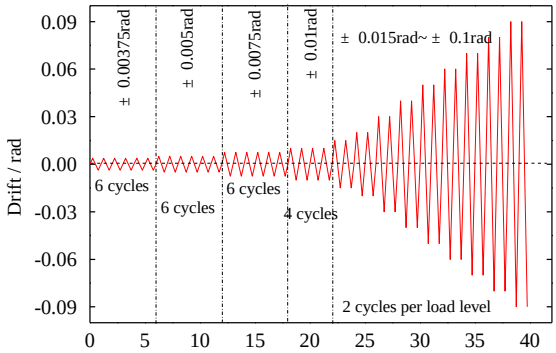

Fig. 5 Loading curve for the cyclic test

Table 2 Material properties of the coupons test

Test samples	Thickness/mm	$\bar{E}$/MPa	$\bar{f}_y$/MPa	$\bar{f}_u$/MPa	$\bar{\delta}$/%
Column flange	15	207233	311.5	484.0	27.2
Column web	10	201800	326.5	498.0	26.7
Beam flange	11	205450	257.0	408.0	27.6
Beam web	7	203813	273.5	409.0	28.2
Web angle	12	201359	244.3	398.7	27.9
Top and seat angle	12	200959	367.7	559.3	29.6
Stiffeners	12	199816	327.7	510.0	28.7

coupons cut from the hot rolled steel beam, column, and angles that used to fabricate the composite specimens. These included 18 steel coupons (three for each column flange, column web, beam flange, beam web, angle, and stiffener) were tested quasi-statically under monotonic tension to obtain the stress-strain curves, the mean values of measured material properties were summarized in Table 2, and in addition, 3 standard concrete cylinders for the concrete slab were prepared and tested on 28th day. The average compression strength of concrete cylinders was 30.8 Mpa.

3. Experimental results

3.1 Analysis of the failure modes

3.1.1 Concrete slab

Each specimen has different failure characteristics due to the different configuration of the specimens the four specimens, while the failure modes of concrete slabs of the composite joints are similar. Fig. 6 shows the development of surface cracks on the concrete floor. Early cracks mainly diffuse along with the four corners of the column at 45

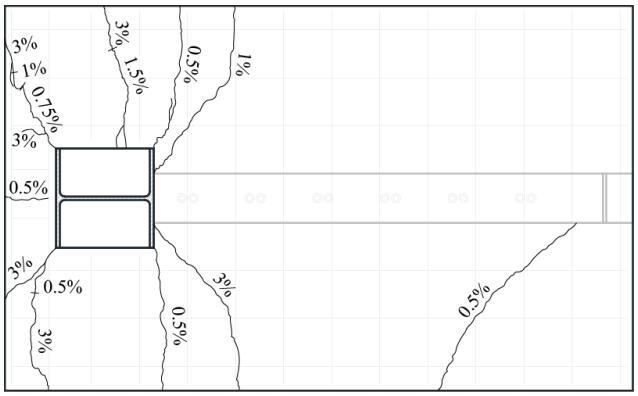

Fig. 6 Crack pattern in the concrete slab of Specimen SJ-1

(a) The failure mode of the concrete in specimen SJ-1 under different drift angle

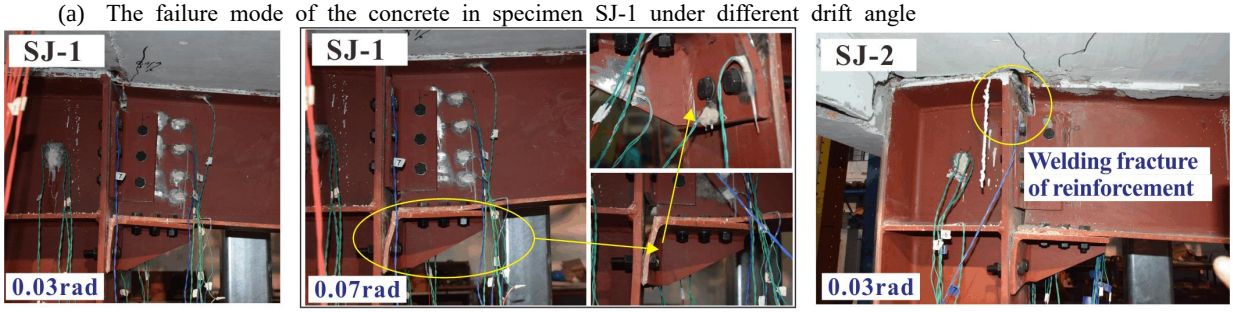

(b) The failure mode of the specimen SJ-1 and SJ-2: cack in seat angle and fracture of reinforcing bar

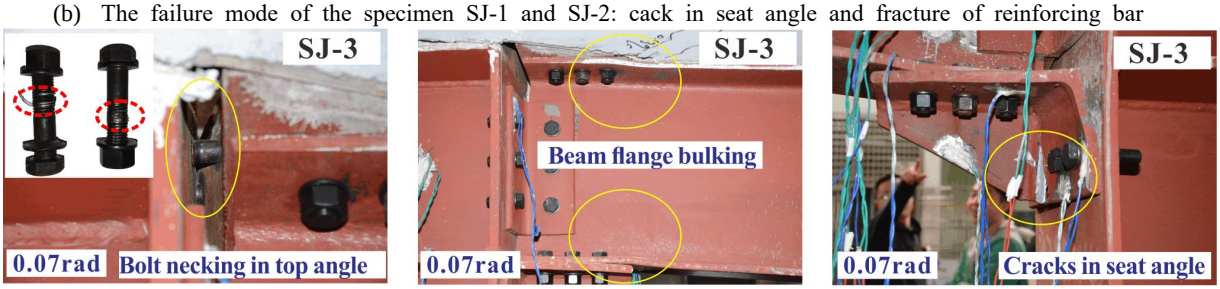

(c) The failure mode of the specimen SJ-3: bolt necking, flange buckling and cracks in seat angle

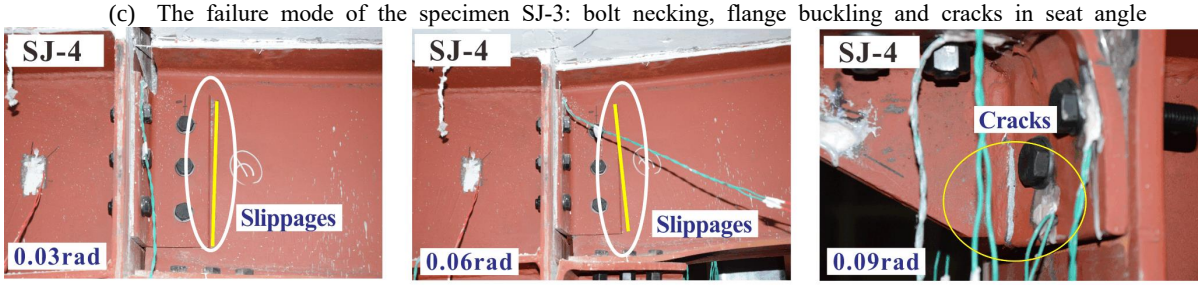

(d) Slippages in specimen SJ-4 and failure of the seat angle

Fig. 7 Failure pattern of the four specimens

degrees. Fig. 7(a) presents the development of the crack in the edge beam. Finally, edge beams failed when two 45-degree inclined cracks were formed under hogging moment in 0.03rad; after that, the concrete floor cannot transmit the tension force produced by hogging moment. This indicated that the anchorage action of the side beam designed in this study could bear a specific tension force at the early stage of the loading process, and then the concrete side beam quieted work due to the failure of oblique cracks, which does not play a role in the whole loading process, especially when the joints enter the elastic-plastic stage. The main reason is that the section dimensions of the side beam are small, and a part of longitudinal reinforcement bars was not anchored in the open part between the two flanges of the column. The concrete in the compression zone of the upper flange of the beam was not crushed until the end of the test under a sagging moment. For the Specimen SJ-2 with 90 degrees bending hook of the longitudinal steel bars welded directly to the flange of the column, the bending point of the hook fractured under the hogging moment at the relative rotation of 0.03 rad.

3.1.2 Large size stiffened angles, web angles, and bolts

As shown in Fig. 7(b), all the short edges of the seat angle cracked at both side of the stiffening rib weld which led to the decrease of the bearing capacity under the action of sagging moment, the test was stopped when the load was reduced to 85% of the peak load, Similar to standard size stiffened angle in the previous study, (Wang *et al*. 2018). It was found that the plastic deformation in the stiffened angle appears obvious bidirectional bending.

In addition, the inner row bolts in seat angle appeared noticeable loosening, and the thread failure was found after these bolts disassembled by hand in the specimens SJ-1, SJ-2, and SJ-3. However, the inner bolts in Specimen SJ-4 with staggered bolts pattern did not appear this phenomenon, and no sign of bolts failure was found after the test. This means the staggered bolts pattern can make the tension force in the inner and outer row bolts more uniform and avoid the failure of the threads caused by the larger low cycle reciprocating tension force in the inner row bolts.

For the Specimen SJ-3 with top angle, a loosening phenomenon caused by the failure of threads of four bolts in top angle was found at the end of the test, the internal bolts had obvious necking under 0.07 rad as shown in Fig. 7(c). The top angle has visible plastic deformation, but there is no fracture around the stiffening rib.

According to the strain monitoring data, the web angle was in the elastic stage before 0.03rad, but a small amount of plastic deformation occurred on the web angles when the test was terminated. The foremost reason is that the tension force required to produce plastic hinges on the web angles was greater than the friction force between the web angle and the beam web. Hence, the slip occured first on the web angles before the bolt fully contacted the web hole. At this stage, the top and seat angles and beam flanges have produced relatively large plastic deformation. Therefore, the web angles mainly played a part when the joint entered the elastic-plastic stage, and it was also the critical component to improve the robustness of joints.

3.1.3 Beam flange and slippage

In all the specimens, the bottom beam flange bucked, as shown in Fig. 7(c), but just the upper beam flange of Specimen SJ-3 with the top angle also bucked. The sections that begin to buckle are all located in the deep bolt holes on the beam flange, which meant that the weakened section of the beam enters the yielding stage during the test.

It can be directly observed that the slippages between the beam flange and the large size angle, the beam web and the web angles were very significant, as shown in Fig 7(d). During the whole loading process, the creaking sound caused by slip always occurred. The ends of the upper and bottom flanges of the beam were directly contacted with the outer surface of the column flange under different load directions. In particular, for the specimens without the top angle under the action of the hogging moment, the clearance between the upper end of the beam flange end and the outer surface of the column flange was about 20 mm.

4. Discussion and evaluation of test results

In general, the behavior of this composite joints has a significant influence on the overall composite frame structural performance, which can be interpreted by the moment-rotation curves, hysteresis loops of each specimen represented by test moment versus story drift angle are shown in Fig. 8, and several essential evaluation indices to measure the performance of the composite joints were summarized in Table 3.

The seismic design specification (ANSI/AISC-341-16 2016) suggests that the composite special moment frame proposes a requirement of story drift angle should not less than 0.04rad. In addition, the calculated flexural moment resistance of connection determined at column face should equal at least 0.8 nominal plastic moment resistance (M_{bp}) of the beam at story drift angle of 0.04rad in composite special moment frame, while the contribution of the concrete in compression is considered in the nominal moment resistance under a sagging moment. As shown in Fig. 8 and Table 3, all the test specimens had a total story drift of at least 0.04 rad with a maximum 15% strength degradation under reverse loading directions, however, only the Specimen SJ-3 which had top and seat large size stiffened angles fulfilled the requirements of the ANSI/AISC-341-16 (2016) It met the requirement of maximum 20% strength degradation until 0.04rad story (under both hogging and sagging moment), while the flexural moment resistance under hogging moment of the other three specimens with none top stiffened angle was less than $0.8M_{bp}$. The main reason is that when the joints were subjected to hogging moments, the concrete had little effect under tension and lacks effective tension components on the tension zone (specimens SJ-1, SJ-2, SJ-4). However, when the joints were subjected to sagging moments, concrete was subjected to compression in the compression zone of the joints, these led to the positive and negative asymmetry of the hysteretic curve, and the bearing capacity of the joints under sagging moments was larger.

The hysteretic loops of the four specimens exhibited significant pinching behavior under cyclic loads, this pinching

effect (the middle part of the outer contour of the hysteretic curve approaches to the origin of the coordinate in different levels) may be due to the relatively obvious slippages between angle leg and beam flange, web angle and beam web. These were observed during the test, and the slip sound accompanied the whole loading process. To a great extent, it reduced the energy absorption capacity of the joints.

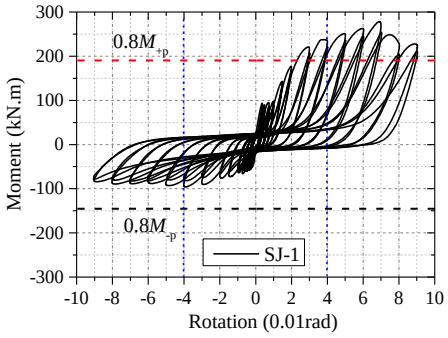

(a) Specimen SJ-1

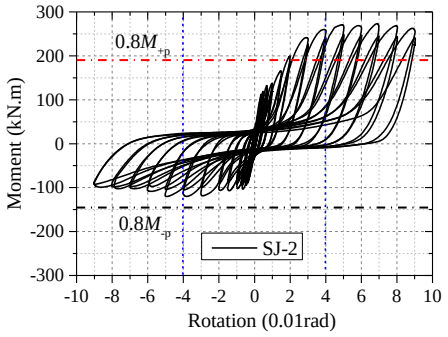

(b) Specimen SJ-2

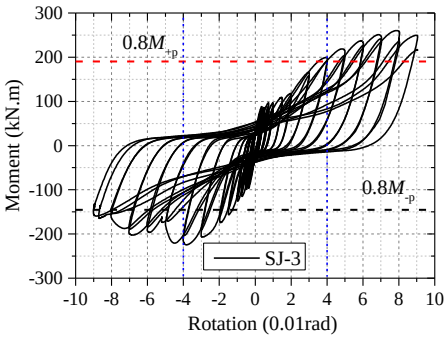

(c) Specimen SJ-3

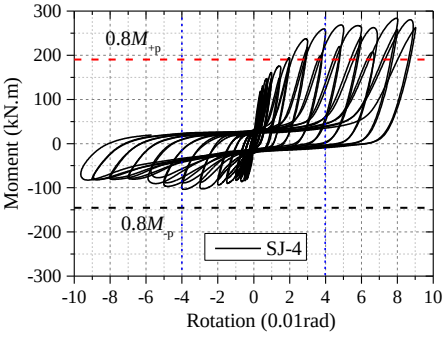

(d) Specimen SJ-4

Fig. 8 Moment versus story drift angle relationships

4.1 Strength and stiffness of the connection

The skeleton curves of the specimens were shown Fig. 9. The peak loads in each loading stage were found in the hysteretic curves. To quantify the mechanical properties of joints, three typical characteristic points based on the moment-rotation skeleton curve are illustrated in Fig. 10, in which yield moment M_y, ultimate moment capacity M_u, and moment at failure stage M_f ($M_f = 0.85M_u$) with the corresponding rotation of θ_y, θ_u, and θ_f are illustrated. The initial rotational stiffness (K_{ini}) was defined as the secant stiffness corresponding to $2/3M_y$.

4.1.1 SJ-1 vs. SJ-2

The welded longitudinal reinforcements on the upper flange of the beam in Specimens SJ-2 can improve the value of initial flexural stiffness under a sagging moment, it had an increment of K_{ini} by 49% and 62% respectively. In terms of yield moment, the effect of the additional weld longitudinal reinforcements can lead to 52% higher M_y under a hogging moment, but it has little effect under the sagging moment for the reason that the additional weld bars were in compression.

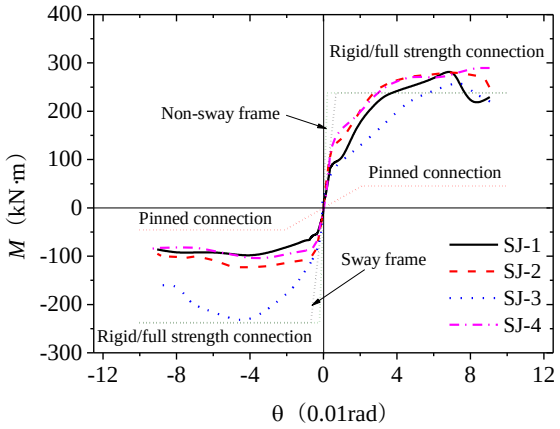

Fig. 9 Skelton curves and classification of the joints

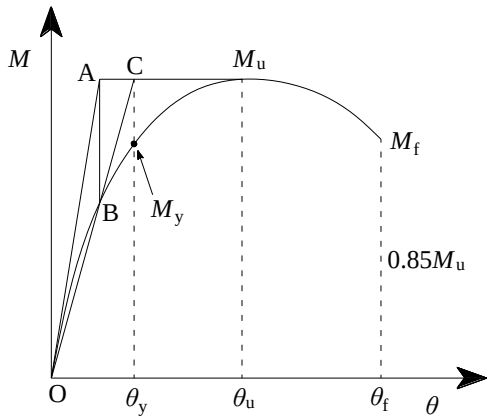

Fig. 10 Definition of yield, ultimate, and failure points

Table 3 Test results of the specimen joints

Specimens	Loading direction	K	M_y	θ_y	M_u	θ_u	M_f	θ_f	μ_θ
SJ-1	-	13210	-69.36	-11.28	-99.91	-40.25	-84.93	-55.53	4.92
	+	18116	225.32	30.38	287.71	68.96	244.55	75.87	2.50
SJ-2	-	21376	-105.73	-7.17	-123.63	-50.33	-105.08	-63.30	8.83
	+	26945	209.34	21.28	283.08	69.16	240.62	90.60	4.26
SJ-3	-	19406	-174.08	-18.98	-236.30	-46.11	-200.85	-70.45	3.71
	+	14128	187.87	36.88	260.90	76.07	221.76	89.60	2.43
SJ-4	-	18807	-87.37	-6.94	-105.18	-40.00	-89.41	-59.58	8.59
	+	26453	195.48	19.61	290.09	80.36	246.58	112.55	5.74

Note: K (kN·m·rad^{-1}), M_y (kN·m), M_u (kN·m), M_f (kN·m), θ_y (10^{-3}rad), θ_u (10^{-3}rad), θ_f (10^{-3}rad)

4.1.2 SJ-1 vs. SJ-3

Compared with Specimen SJ-1, the hogging yield moment and the ultimate moment of specimen SJ-3 were increased by 151% and 136%, respectively. Due to a top angle of the same size as the large size stiffened seat angle was added in Specimen SJ-3. However, it was found that the sagging yield moment and the ultimate moment of specimens SJ-3 to SJ-1 decreased slightly, the main reason was that concrete was not covered on the top angle. It is shown that under a sagging moment, the compression concrete on the upper beam flange was more effective in the sagging moment resistance than that of large size stiffened angle.

4.1.3 SJ-1 vs. SJ-4

Compared with Specimen SJ-1, the initial rotational stiffness of the specimen SJ-4 was increased by 42% under a sagging moment and 46% under hogging moment. However, for the sagging and hogging moment, the increased range was less than 5%. The staggered bolts can change the failure mode of the joints and improve the ductility of the joints, which will be discussed in detail in the following section.

4.2 Rotational capacity and ductility

The ductility of specimens is defined by the ability of elastic-plastic deformation of specimens without noticeable reduction of bearing capacity. In general, the ductility of specimens is expressed by the ductility coefficient μ_θ, which is determined by the ratio of the failure rotation θ_f (corresponding to the rotation when the peak moment of the specimens drops to 85%) to the yield rotation θ_y. The ductility coefficients μ_θ of the specimens were shown Table 3, and the other rotation indexes are defined in Fig. 10

$$\mu_\theta = \theta_d / \theta_y \tag{1}$$

It can be seen that the ultimate rotation θ_u under sagging moment was more than 0.04 rad (0.04 rad$\le\theta_u\le$0.05 rad) rad and the hogging moment is larger than 0.069 rad (0.069 rad$\le\theta_u\le$0.08 rad), especially, it can reach 0.08rad in Specimen SJ-4. This indicated that all specimens have sufficient rotational capacity. Table 3 shows that the ductility coefficients μ_θ of the specimens SJ-2 and SJ-4 in the positive and negative directions exceed 4.0, which demonstrated that the welding reinforcement bar and staggered bolt pattern enhanced the ductility of this type joint.

4.3 Energy dissipation capacity

Energy dissipation capacity of joints is an essential index of structural resistance to seismic hazard. The total energy dissipation capacity is defined as the envelope area of the hysteretic curve. In addition, energy dissipation capacity of structures or components can usually be evaluated by dimensionless equivalent viscous damping (*EVD*) h_e is defined in Eq. (2) and Fig. 11, $S_{ABD} + S_{BCD}$ is the energy dissipated by the structure or component through a loading cycle; $S_{OAE} + S_{OCF}$ is the triangular energy corresponding to the maximum bearing capacity of the structure or part under the same load.

$$h_e = \frac{1}{2\pi}\frac{S_{ABD}+S_{BCD}}{S_{OAE}+S_{OCF}} \tag{2}$$

Fig.12 describes the changes of equivalent viscous damping. The *EVD* of the four specimens increased with the rotation angle.

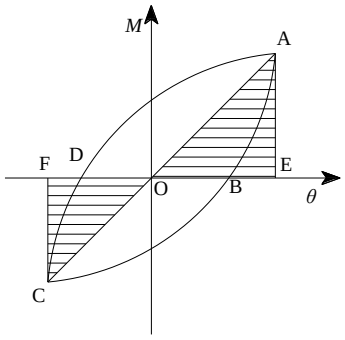

Fig. 11 Definition of a hysteretic loop

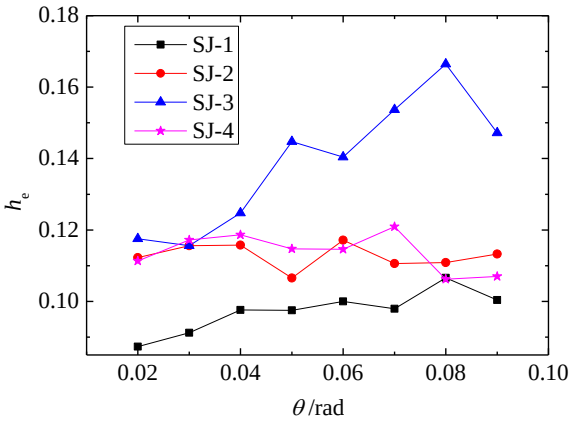

Fig. 12 Equivalent viscous damping

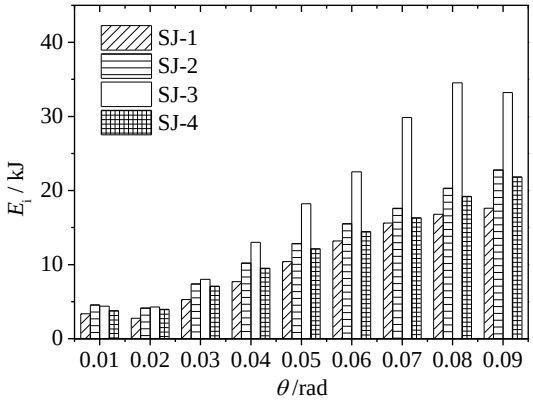

Fig. 13 Energy dissipated during in each step

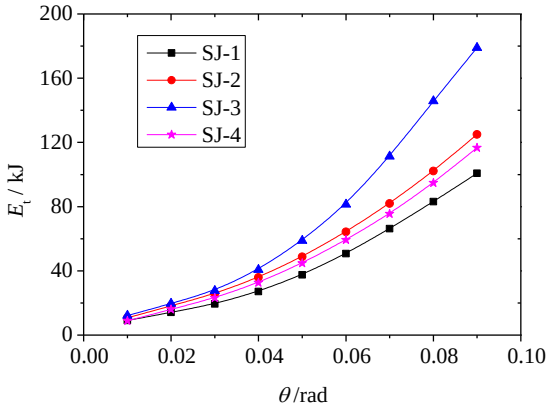

Fig. 14 Accumulated energy dissipation

However, it was relatively small, less than 0.25, due to the severe pinching effect caused by sliding. The *EVD* increases obviously with adding the large size top stiffened angle. Another two properties, namely, energy dissipated in each step (E_i), accumulated energy dissipation (E_t). Figs. 13 and 14 show the E_i and E_t of the four specimens, The accumulated energy dissipations of the specimens at failure varied from 100 kJ to 180 kJ, the Et of specimen SJ-3 at 0.06rad was almost 1.6 times that of Specimen SJ-1, meanwhile, it was found that the larger rotation was, the more obvious the energy dissipation effect achieved at each stage for Specimen SJ-3. Therefore, the presence of the large size top stiffened angle could highly enhance energy dissipation behavior, however, in comparison of specimens SJ-2 and SJ-3, the increase caused by welding longitudinal reinforcement and applying staggered bolt pattern was slight when compared with that of Specimen SJ-1.

4.4 Classification by connection rigidity and strength

The connection rigidity and strength can be classified by CEN-1993-8 (2005) base on the characteristic of their moment-rotation curves, for the perspective of joint rigidity, a joint can be evaluated as nominally pinned, rigid or semi-rigid by its initial rotational stiffness ($S_{j.ini}$) according to the criteria suggested by CEN-1993-8 (2005) : A joint is nominally pinned if the $S_{j.ini} \leq 0.5EI/L$, where E, I and L are elasticity modulus, second moment of area, and the length of the steel beam, respectively. A joint is rigid if the $S_{j.ini} \geq kEI/L$, k=25 for none braced frame and k= 8 for the braced frame. In terms of strength, the minimum required connection resistance for partial-strength design is $0.25M_{bp}$, and the full-strength connection resistance is beyond M_{bp} (M_{bp} is the beam cross-section plastic moment).

The skeleton envelope of the four specimens is identified by boundaries of rigidity and strength as illustrated in Fig. 9. It indicates that all four types of joints can be considered as semi-rigid joints, either in none braced frame or braced frames. The Specimen SJ-3 with both large sizes stiffened top and seat angles can be regarded as full-strength joint either in hogging or sagging moment; the other three connections (Specimens SJ-1, SJ-2 and SJ-4) were full strength connection in sagging moment and partial strength in the hogging moment.

5. Conclusions

In this study, the large-size exterior composite TSDW joints were tested under cyclic loading conditions. The vital parameters that affected the seismic performance of the joints were designed, and their effects were discussed in detail. The following conclusions can be drawn based on the results of the experimental investigations in this study:

The hysteretic curves of large-size exterior composite TSDW joints showed noticeable pinching effect, which was mainly due to the obvious slip effect of web angles and large-size angles subjected to horizontal shear.

The failure modes of large-size angle composite joints without staggered bolts under cyclic loading included the interaction failures of edge beam, beam flange buckling, screw thread failure, biaxial bending deformation of large-size angle and fracture around the stiffening ribs.

The welding between longitudinal reinforced bars on the upper flange of the beam and the flange of the column can effectively improve the stiffness, bending capacity and ductility of the joints under hogging moment, when compared with the behavior of other specimens.

The staggered bolt pattern can avoid the screw thread failure of inner bolts under cyclic loading, which in turn improved the stiffness and ductility of the joint under sagging moment significantly, and slightly improved the energy dissipation capacity. However, it had limited enhancement of the bending capacity.

The edge beams of side column joints played an essential role in the early stage of loading only. It quitted work quickly after two oblique cracks appeared. The concrete in the compressive zone of the joint area was more effective than large size stiffened angle in improving the stiffness and bending capacity of the joint.

Despite neglecting the contact between column flange and compressive concrete, when top and seat angles were adopted, it can still meet the seismic requirements of special moment resist steel frames in American seismic design code ANSI/AISC-341-16, as the inter-story displacement drift was higher than 0.04 rad, and the corresponding bending moment is greater than the required 0.8 M_{bp}.

Acknowledgments

This study was supported by National Natural Science Foundation of China (Grant No. 51778241; 51638009; 51978279), the Fundamental Research Funds for the Central Universities (Grant No. 2019MS121; 2019PY20; 2019ZD47), Chinese Postdoctoral Science Foundation (Grant No. 2019M652898) and Guangdong Basic and Applied Basic Research Foundation (2020A1515011307).

References

Abdalla, K.M., Drosopoulos, G.A. and Stavroulakis, G.E. (2015), "Failure Behavior of a Top and Seat Angle Bolted Steel Connection with Double Web Angles", *J. Struct. Eng.*, **141**(7). https://doi.org/10.1061/(asce)st.1943-541x.0001132.

Amadio, C. and Fragiacomo, M. (2003), "Analysis of rigid and semi-rigid steel-concrete composite joints under monotonic loading Part I: Finite element modelling and validation", *Steel Compos. Struct.*, **3**(5), 349-369. https://doi.org/10.12989/scs.2003.3.5.349.

ANSI/AISC-341-16 (2016), Seismic provisions for Structural Steel Buildings. American Institute of Steel Construction. Chicago.

Artar, M. and Daloglu, A.T. (2015), "Optimum design of composite steel frames with semi-rigid connections and column bases via genetic algorithm", *Steel Compos. Struct.*, **19**(4), 1035-1053. https://doi.org/10.12989/scs.2015.19.4.1035.

Brunesi, E., Nascimbene, R. and Rassati, G.A. (2014), "Response of partially-restrained bolted beam-to-column connections under cyclic loads", *J.Constr. Steel Res.*, **97**, 24-38. https://doi.org/10.1016/j.jcsr.2014.01.014.

CEN-1993-8 (2005), Eurocode 3: Design of steel structures. Part 1-8: Design of Joints. European Committee for Standardization. Brussels.

Citipitioglu, A.M., Haj-Ali, R.M. and White, D.W. (2002), "Refined 3D finite element modeling of partially-restrained connections including slip", *J. Constr. Steel Res.*, **58**(5-8), 995-1013. https://doi.org/10.1016/s0143-974x(01)00087-6.

Garlock, M.M., Ricle, J.M. and Sause, R.(2003), "Cyclic load tests and analysis of bolted top-and-seat angle connections", *J. Struct. Eng.*, **129**(12), 1615-1625. https://doi.org/10.1061/(ASCE)0733-9445(2003)129:12(1615).

GB50017-2017 (2018), Standard for design of steel structures. Beijing, China Architecture and Building Press.

Gil, B. and Bayo, E. (2008), "An alternative design for internal and external semi-rigid composite joints. Part I: Experimental research", *Eng. Struct.,* **30**(1), 218-231. https://doi.org/10.1016/j.engstruct.2007.03.009.

Gil, B., Goni, R. and Bayo, E. (2013). "Experimental and numerical validation of a new design for three-dimensional semi-rigid composite joints", *Eng. Struct.*, **48**, 55-69. https://doi.org/10.1016/j.engstruct.2012.08.034.

Hantouche, E.G. and Mouannes, E.N. (2016), "Strength and stiffness modeling of extended endplate connections with circular and rectangular bolt configurations", *Steel Compos.Struct.*, **22**(2), 323-352. https://doi.org/10.12989/scs.2016.22.2.323.

Kiamanesh, R., A. Abolmaali and M. Razavi. (2013). "Effect of Circular Bolt Pattern on Behavior of Extended End-Plate Connection", *J. Struct. Eng.* **139**(11): 1833-1841. https://doi.org/10.1061/(asce)st.1943-541x.0000765.

Kumar, S.R.S. and Smitha, M.S. (2013), "Steel–concrete composite flange plate connections: Cyclic performance and tests", *J. Constr. Steel Res.*, **83**(3), 216-222. https://doi.org/10.1016/j.jcsr.2013.01.003.

Lee, C.H., Jung, J.H., Kim, S.Y. and Kim, J.J. (2016), "Investigation of Composite Slab Effect on Seismic Performance of Steel Moment Connections", *J. Constr. Steel Res.*, **117**, 91-100. https://doi.org/10.1016/j.jcsr.2015.10.004.

Lee, S.S. and Moon, T.S. (2002), "Moment-rotation model of semi-rigid connections with angles", *Eng. Struct.*, **24**(2), 227-237. https://doi.org/10.1016/s0141-0296(01)00066-9.

Ma, H., Wang, J., Lui, E.M., Wan, Z. and Wang, K. (2019), "Experimental study of the behavior of beam-column connections with expanded beam flanges", *Steel Compos. Struct.*, **31**(3), 319-327. https://doi.org/10.12989/scs.2019.31.3.319.

Meng, B., Zhong, W. and Hao, J. (2018), "Anti-progressive collapse behavior of beam-to-column assemblies with bolted-angle connections under different span ratios", *Adv. Struct Eng.*, **21**(6), 891-905. https://doi.org/10.1177/1369433217734636.

Pirmoz, A., Khoei, A.S., Mohammadrezapour, E. and Daryan, A.S. (2009), "Moment-rotation behavior of bolted top-seat angle connections", *J. Constr. Steel Res.*, **65**(4), 973-984. https://doi.org/10.1016/j.jcsr.2008.08.011.

Reinosa, J.M., Loureiro, A., Gutierrez, R. and Lopez, M. (2015), "Analytical plate approach for the axial stiffness prediction of stiffened angle cleats", *J. Constr. Steel Res.*, **106**, 77-88. https://doi.org/10.1016/j.jcsr.2014.12.010.

Reinosa, J.M., Loureiro, A., Gutierrez, R. and Lopez, M. (2019), "Mechanical stiffness prediction of beam-to-column stiffened angle joints", *J. Constr. Steel Res.*, **105875**. https://doi.org/10.1016/j.jcsr.2019.105875.

Wang, J., Lu, J., Zhang, H. and Zhao, C. (2018), "Experimental investigation on seismic performance of endplate composite joints to CFST columns", *J. Constr. Steel Res.*, **145**, 352-367. https://doi.org/10.1016/j.jcsr.2018.03.006.

Wang, P. (2018), "Study on Mechanical Behaviors of Beam-to-Column Connection with Stiffened Top and Seat Angles", Ph.D. Dissertation. South China University of Technology. Guangzhou..

Wang, P., Pan, J., Wang, Z. and Chen, S. (2018), "Experimental and analytical behavior of stiffened angle joints", *Steel Compos. Struct.*, **26**(1), 67-78. https://doi.org/10.12989/scs.2018.26.1.067.

Xiao, Y., Choo, B. and Nethercot, D. (1994), "Composite connections in steel and concrete. I. Experimental behaviour of composite beam—Column connections", *J. Constr. Steel Res.*,

31(1), 3-30. https://doi.org/10.1016/0143-974X(94)90021-3.
Yuan, Z., Tan, K.H. and Ting, S.K. (2011), "Testing of composite steel top-and-seat-and-web angle joints at ambient and elevated temperatures, Part 1: Ambient tests", *Eng. Struct*., **33**(10), 2727-2743. https://doi.org/10.1016/j.engstruct.2011.04.027.

CC